6.5 Propellers of Minimum Induced Loss, and Water Tunnel Tests of Such a Propeller

E. E. Larrabee
Massachusetts Institute of Technology

Abstract

The fundamental vortex theory for a single rotation propeller with a finite number of blades is reviewed. The theory leads to the specification of a radial distribution of bound circulation on each blade for minimum induced loss, analogous to the elliptic spanwise distribution of bound circulation on a wing for minimum induced drag. A propeller designed in accord with this theory has been tested in the water tunnel at M.I.T.'s Marine Hydrodynamics Laboratory where it exhibited high efficiency in spite of localized cavitating flow. A knowledge of the flow field for an optimum propeller is of value to the airframe designer seeking to maximize the performance of the airplane-propeller combination.

Figure 1 presents the geometry of the force and velocity components associated with the operation of a representative blade element. The fluid velocity W at the blade element is made up of the flight, or advance velocity, V, the rotational velocity, Ωr, and the induced, or "inflow" velocity w_i. The induced velocity is customarily resolved into an axial component aV and a rotational component $a'\Omega r$. The elementary force dF is resolved into lift and drag components dL and dD where the angle ϵ, defined as $\tan^{-1}(c_d/c_\ell)$, is an angle determined by blade profile characteristics in two dimensional flow at the appropriate Reynolds number, as in lifting line theory.

The blade element efficiency is given by

$$\eta_{element} = \frac{VdT}{\Omega dQ} = \frac{V}{\Omega r}\,\frac{dF\cos(\phi_i+\epsilon)}{dF\sin(\phi_i+\epsilon)} \qquad 1$$

and since

$$\tan\phi_i = \frac{V(1+a)}{\Omega r(1-a')} \qquad 2$$

while

$$\tan(\phi_i+\varepsilon) = \frac{\sin(\phi_i+\varepsilon)}{\cos(\phi_i+\varepsilon)} \qquad 3$$

it follows that

$$\eta_{element} = \frac{\tan\phi_i}{\tan(\phi_i+\varepsilon)} \times \frac{1-a'}{1+a} = \eta_{profile} \times \eta_{induced} \qquad 4$$

In this discussion I will be mainly concerned with the "induced" efficiency $(1-a')/(1+a)$.

Figure 2 presents the geometry of the velocity field in the propeller slipstream. An elementary helical vortex filament is convected normal to itself with velocity w by the induced velocities of all the vortex filaments lying in the approximately helicoidal vortex sheets trailed by each of the propeller blades. The vortex velocity w, which is the same as the local slipstream velocity, may be resolved into axial and rotational (or "tangential") velocity components w_a and w_t, respectively.

If the filament helix angle is ϕ, the filament will appear to move with an axial velocity v', which might be due either to real axial velocity w_a or to real rotational velocity w_t (like the rotating stripes on a barber pole); but since it is a vortex filament, and can only move normal to itself,

$$w_a = v' \cos^2\phi, \text{ and} \qquad 5$$

$$w_t = v' \cos\phi \sin\phi \qquad 6$$

Figure 3 presents the so called "lightly loaded" propeller relations between velocities w_a and w_t in the slipstream at radius r and the corresponding inflow velocity components aV and $a'\Omega r$ at the propeller disc. Since the propeller is lightly loaded, the trailing vortex helix angle ϕ in the slipstream at radius r is indistinguishable from the angle $\tan^{-1}(V/\Omega r)$ at the propeller blade element at the same radius. Following momentum theory the inflow velocities are taken as half their values in the developed slipstream:

$$a = \frac{1}{2}\frac{w_a}{V} = \frac{1}{2}\left(\frac{v'}{V}\right)\frac{\Omega^2r^2}{\Omega^2r^2+V^2} \qquad 7$$

$$a' = \frac{1}{2}\frac{w_t}{\Omega r} = \frac{1}{2}\left(\frac{v'}{V}\right)\left(\frac{V^2}{\Omega^2r^2+V^2}\right) \qquad 8$$

The induced efficiency of a blade element

$$\eta_{induced} = \frac{1-a'}{1+a} \cong \frac{1}{1+a'+a} = \frac{1}{1+\frac{1}{2}(\frac{v'}{V})} \qquad 9$$

may thus be expressed in terms of the apparent axial velocity of the slipstream, v', which up to now has been considered to be an arbitrary function of r. Betz showed in 1919 that $\eta_{induced}$ for the propeller as a whole is maximized if $\eta_{element}$ is the same for all blade elements, that is, if v'/V is independent of r. If v' is independent of r, all vortex filaments in a helicoidal vortex sheet appear to move axially as a rigid surface, although this is not actually the case, since w_a and w_t are given by eqs. 5 and 6.

Since circulation cannot be added to the flow in the slipstream, it follows that the circulation within a slipstream tube of radius r

$$\Gamma = 2\pi r w_t \qquad 10$$

must comprise the total circulation of the helical vortex filaments trailed by each of the B blades of the propeller, an amount equal to the total bound vorticity at the radius r. The bound vorticity on each blade at radius r is then

$$\Gamma(r) = \frac{2\pi r w_t}{B} = \frac{2\pi}{B}\frac{Vv'}{\Omega}\frac{\Omega^2 r^2/V^2}{(\Omega^2 r^2/V^2)+1} \qquad 11$$

or

$$\frac{B\Omega\Gamma(r)}{2\pi V v'} = \frac{x^2}{x^2+1} \qquad 11a$$

where $x \equiv \Omega r/v$.

Since, B, Ω, 2π, V, and v' are all constants for a minimum induced loss propeller, $B\Omega\Gamma(r)/2\pi Vv' = x^2/(x^2+1)$, can be regarded as a normalized form for the bound circulation, $\Gamma(r)$, expressed as a function of the normalized radial coordinate, $x = \Omega r/V$. Alternatively, the quantity $x^2/(x^2+1)$, which is also equal to $\cos^2\phi$, may be regarded as the ratio of the axial velocity in the slipstream to the apparent velocity, w_a/v'. Figure 4 presents the normalized radial circulation distribution (or the w_a/v' ratio) as a function of the normalized radial coordinate, x. The ratio of the rotational velocity in the slipstream to the apparent velocity w_t/v', equal to $x/(x^2+1)$, is given for comparison. It is seen that single rotation propellers of minimum induced loss inevitably have appreciable slipstream swirl near

the center of the slipstream where ϕ is large; the swirl angle in airplane coordinates being given approximately by $\tan^{-1}[w_f/(V+w_a)]$.

Strictly speaking, eqns. 7-11a apply to a propeller with so many blades that the spacing between the individual vortex sheets in the slipstream is small compared to r, called the $B\to\infty$ case. Since actual propellers have a small number of blades and may operate at large helix angles, which also tends to increase the spacing between vortex sheets (note that $\eta_{profile} = \tan\phi_i/\tan(\phi_i+\epsilon)$ is maximized when $\phi_i = \pi/4 - \epsilon/2$), it is necessary to account for the reduction in the average rotational velocity between vortex sheets in the developed slipstream (compared to the $v' \cos\phi \sin\phi$ value at the sheets themselves) when calculating the circulation.

Figure 5 shows Prandtl's approximate solution to this problem. He assumed that the flow near the edges of the helicoidal vortex sheets in the slipstream is like the two dimensional flow near the edges of a semi-infinite array of flat plates moving with velocity v. The average velocity of the fluid between the plates is given by the fraction $F = (2/\pi)\cos^{-1} e^{-f}$ times v, where $f = \pi(\xi/s)$ is a dimensionless measure of the distance ξ from the edge of the plates spaced a distance s apart. The corresponding edge distance function for the helicoidal vortex sheets is

$$f = \frac{B(1-\lambda x)\sqrt{1+\lambda^2}}{2\lambda} \qquad 12$$

where $\lambda = V/\Omega R$ is an advance ratio based on the flight velocity V and the rotational tip speed ΩR. The quantity F is interpreted as the ratio of the average rotational velocity in the slipstream at radius r to the rotational velocity near the sheets, $v'\sin\phi\cos\phi$, or, what is the same thing, the ratio of the bound circulation at radius r for a propeller with a finite number of blades to the corresponding circulation for $B\to\infty$.

Figure 6 presents representative examples of the radial distribution of bound circulation for a minimum induced loss three blade propeller operating at two advance ratios, $\lambda = 1/5$ and $\lambda = 2/3$, corresponding to climbing and cruising flight conditions, respectively, where F has been calculated according to Prandtl's rule. These optimum radial circulation distributions for propeller blades loaded so as to produce constant apparent velocity of the helicoidal vortex sheets in the slipstream, independent of the radius, correspond to the elliptic spanwise distribution of circulation for a wing, loaded so as to produce constant downwash velocity at the trailing vortex sheet in the wing wake, independent of a spanwise coordinate.

Although an untwisted wing of elliptic planform gives an elliptic spanwise

circulation distribution for all angles of attack within the linear range of section lift coefficient versus angle of attack, there is no corresponding propeller blade planform that gives the optimum radial circulation distribution for all advance ratios. Figure 8 presents plots of $(\Omega/\pi v')cc_\ell$ versus $\lambda x = r/R$ for three bladed propellers of minimum induced loss operating at the two advance ratios given on Figure 7. If the section lift coefficient, c_ℓ, is considered constant for all values of r/R, the curves may be interpreted as plots of the optimum radial chord distribution. It is seen that a propeller optimized for a low advance ratio needs blades with a wide chord inboard where the airspeed is low, and a narrow chord outboard where the airspeed is high. A propeller optimized for large advance ratios, on the other hand, will require a more elliptic distribution of chord since the blade element airspeeds are not so strongly dependent on the radial coordinate. In any event, it is seen that a propeller can only be optimized at one advance ratio and that a general theory of non-optimum propellers will be required to calculate propeller performance away from the design point.

A traditional method for doing this was developed by Glauert. In his scheme the differential increases in axial and rotational momentum in an annular element of slipstream of radius r and width dr are set equal separately to the thrust and torque components of the airload acting on each of the B blade elements, thus:

$$\frac{dT}{dr} = 2\pi\rho rV(1+a)2aV = \frac{1}{2}\rho W^2 BcC_y \qquad 13$$

and

$$\frac{1}{r}\frac{dQ}{dr} = 2\pi\rho rV(1+a)2a'r\Omega = \frac{1}{2}\rho W^2 BcC_x \qquad 14$$

where

$$C_y = c_\ell \cos\phi_i - c_d \sin\phi_i \qquad 15$$

$$C_x = c_\ell \sin\phi_i + c_d \cos\phi_i \qquad 16$$

Equations 13 and 14 are adapted for calculation by solving 13 for a and 14 for a', where σ is the local solidity, $Bc/2\pi r$:

$$\frac{a}{a+1} = \frac{\sigma C_y}{4 \sin^2\phi_i} \qquad 13a$$

$$\frac{a'}{1-a'} = \frac{\sigma C_x}{4 \sin\phi_i \cos\phi_i} \qquad 14a$$

An iterative procedure is employed at each of several blade radial stations whereby blade element angles of attack are assumed giving c_ℓ and c_d (airfoil properties),

$\phi_i = \beta - \alpha$ (β is the blade angle),

C_y and C_x (eqs. 15 and 16),

a and a' (eqs. 13a and 14a),

and finally

$$\phi_i = \tan^{-1}\left(\frac{V}{\Omega r}\right)\left(\frac{1+a}{1-a'}\right)$$

for each assumed value of α. The iteration is terminated when $\phi_i = \beta - \alpha = \tan^{-1}\left(\frac{V}{\Omega r}\right)\left(\frac{1+a}{1-a'}\right)$ and the converged values of C_y and C_x are then suitably integrated radially to yield the propeller thrust and torque (or power).

Equations 13 and 14 depend on the absence of radial flow in the slipstream, the very thing that Prandtl's vortex sheet spacing correction was intended to account for in the case of a propeller operating with minimum induced loss. Glauert in his article in Durand's "Aerodynamic Theory" (1934) suggested modifying Eqs. 13a and 14a to read

$$\frac{a}{1+a} = \frac{\sigma C_y}{4 \sin^2\phi_i F} \qquad 13b$$

$$\frac{a'}{1-a'} = \frac{\sigma C_x}{4 \sin\phi_i \cos\phi_i F} \qquad 14b$$

(there is a misprint in the book whereby the quantity F appears in the numerator of the right hand side of eqns. 13b and 14b instead of the denominator). Goldstein, in his doctor's thesis (published as "On the Vortex Theory of Screw Propellers" in the Proceedings of the Royal Society (A) 123, 440 1929) refined Prandtl's value for F by considering the flow about moving helicoidal surfaces of B sheets per turn rather than an array of moving flat plates. F. N. Lock proposed an alternative scheme based on Goldstein's values for F (Lock calls them $\mathcal{L}$, sometimes read "kappa") in which the momentum balance of eqns 13 and 14 is abandoned and the inflow velocity, w_i, (Fig. 1) is considered to be normal to the resultant velocity at the blade element, W. The inflow velocity, in turn, is considered to be half the developed slipstream velocity increment, w, given by a form of eq. 10:

$$B\Gamma(r) = 2\pi r(w \sin\phi)F \qquad 10b$$

Lock's procedure would be identical to Glauert's modified scheme if the blade elements had no drag. Theodorsen introduced a correction to Lock's procedure to allow for slipstream contraction; he also verified Goldstein's F values by rheo-electric analog computation, and extended them to the case of intersecting helicoidal vortex sheets, as would be trailed by a counterrotating propeller. Lock's method has recently been reviewed by Pauling ("The Effects of Uncertainties on Predicting Rotor and Propeller Performance", Pennsylvania State University report PSU AERSP 75-3) who wrote a digital computer program to carry out a version of Lock's procedure with several optional features, including a slipstream contraction effect. I personally am bothered by the fact that all of these non-optimum propeller theories depend on Prandtl or Goldstein F values, which are calculated on the assumption of trailing vortex sheet geometry appropriate to a propeller of minimum induced loss. The procedures are analogous to an approximate lifting line wing theory in which the two dimensional lift on a chordwise element is corrected by $[1-(2y/b)^2]^{1/2}$ to account for three dimensional flow effects.

Figure 9 presents a marvelous smoke flow visualization photograph of the operation of a two bladed propeller obtained by Prof. F. N. Brown at Notre Dame. The helicoidal vortex sheets are seen to roll up rather rapidly as they are left behind in the slipstream by the propeller blades, exactly in the way that the trailing vortex sheet left behind a wing does. The picture suggests that the propeller is not optimally loaded because there is perhaps not enough axial motion of the inboard portions of the trailing vortex sheets--although this is difficult to judge, because the sheet is marked by smoke particles which have <u>both</u> rotational as well as axial velocities, while the "apparent" v' of the theory specifies the motion of the helicoidal <u>surfaces</u> past a fixed point; for example, the "apparent" axial velocity v' component due to "barber pole" helix rotation, $v'_{bp} = w_t \tan\phi$, does not show in the picture.

I will conclude this presentation of propeller theory with the observation that the propeller equivalent of lifting line theory does not exist, and that all propeller computation procedures contain some element of empiricism. Helicopter aerodynamicists have had some success in the application of machine based discrete vortex models to the prediction of rotor characteristics; see for example Landgrebe's "The Wake Geometry of a Hovering Helicopter Rotor and its Influence on Rotor Performance" (Journal of the American Helicopter Society, Vol 17, no. 4, October 1972), but in my opinion work still needs to be done.

Figure 10 shows a research propeller constructed at M.I.T. for testing in the water tunnel of the Marine Hydrodynamic Laboratory. The propeller was designed to have two blades of a minimum induced loss geometry appropriate in an application to a direct drive 1700cc Volkswagen engine installation which develops 47 hp at 3800 rpm at sea level. The full scale propeller would have a diameter of 50 inches and be optimized at 120 mph, giving an advance ratio $J = V/nD = 0.667$ ($\lambda = 0.212$). The model propeller had a diameter of 12 inches and was constructed so it could be tested either in a four blade or a two blade version, since additional blades could be readily made once the milling machine cam had been constructed to make one blade.

Figure 11 shows the propeller operating near its design advance ratio in the water tunnel at a pressure low enough to cause appreciable cavitation over the outer quarter of the blades. Note that the propeller is tested in a pusher configuration with the shaft extending upstream into the tunnel stilling section, and with a spinner fitted downstream to preserve good flow at the inboard blade stations. The compound helical character of the cavitation marked tip vortex core is noteworthy.

Figure 12, finally, presents the measured characteristics of this propeller as tested in the water tunnel at a loading high enough to produce light cavitation. The effects of cavitation are seen in the upward bulge and the downward dip of the torque and thrust curves, respectively. The peak efficiency of 85%, obtained at an advance ratio, $J = 0.8$, is the highest ever measured in this tunnel.

It is hoped that this paper will encourage general aviation aerodynamicists to seek propeller geometries better suited to the operation of their own airplanes than the compromise production propellers available as off-the-shelf items. It should be borne in mind that the interference flows produced at the propeller by a large fuselage downstream need to be taken into account in the design of an actual propeller, and that efficient propellers inevitably create large slipstream swirl components on the fuselage nose and flanks which should be considered in the design of engine air inlets, carburetor air scoops, exhaust stacks, landing gear struts, and even door handles.

w_i = induced, or inflow velocity at propeller

α_i = induced angle of attack

β = nominal blade angle

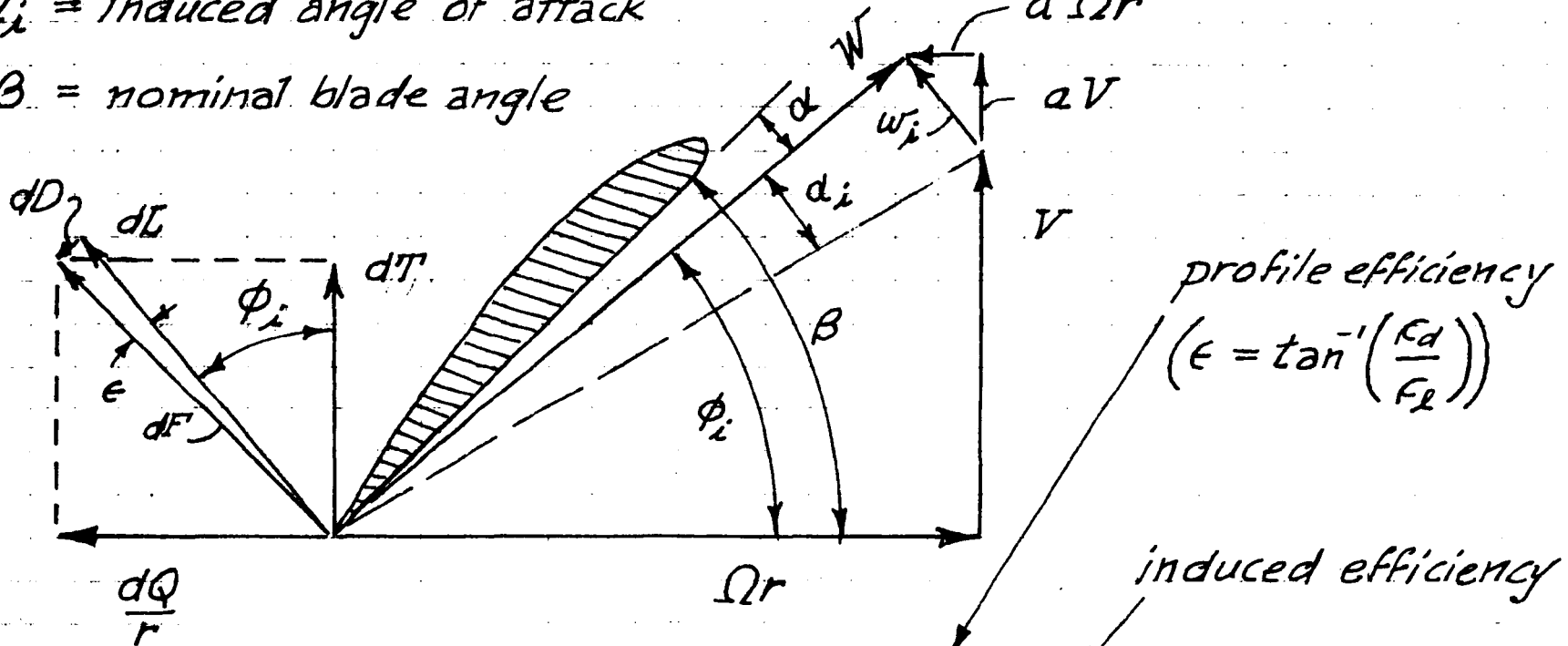

$$\eta = \frac{V\,dT}{\Omega\,dQ} = \left[\frac{\tan\phi_i}{\tan(\phi_i+\epsilon)}\right]\cdot\left[\frac{1-a'}{1+a}\right]$$

Figure 1. Blade Element Geometry

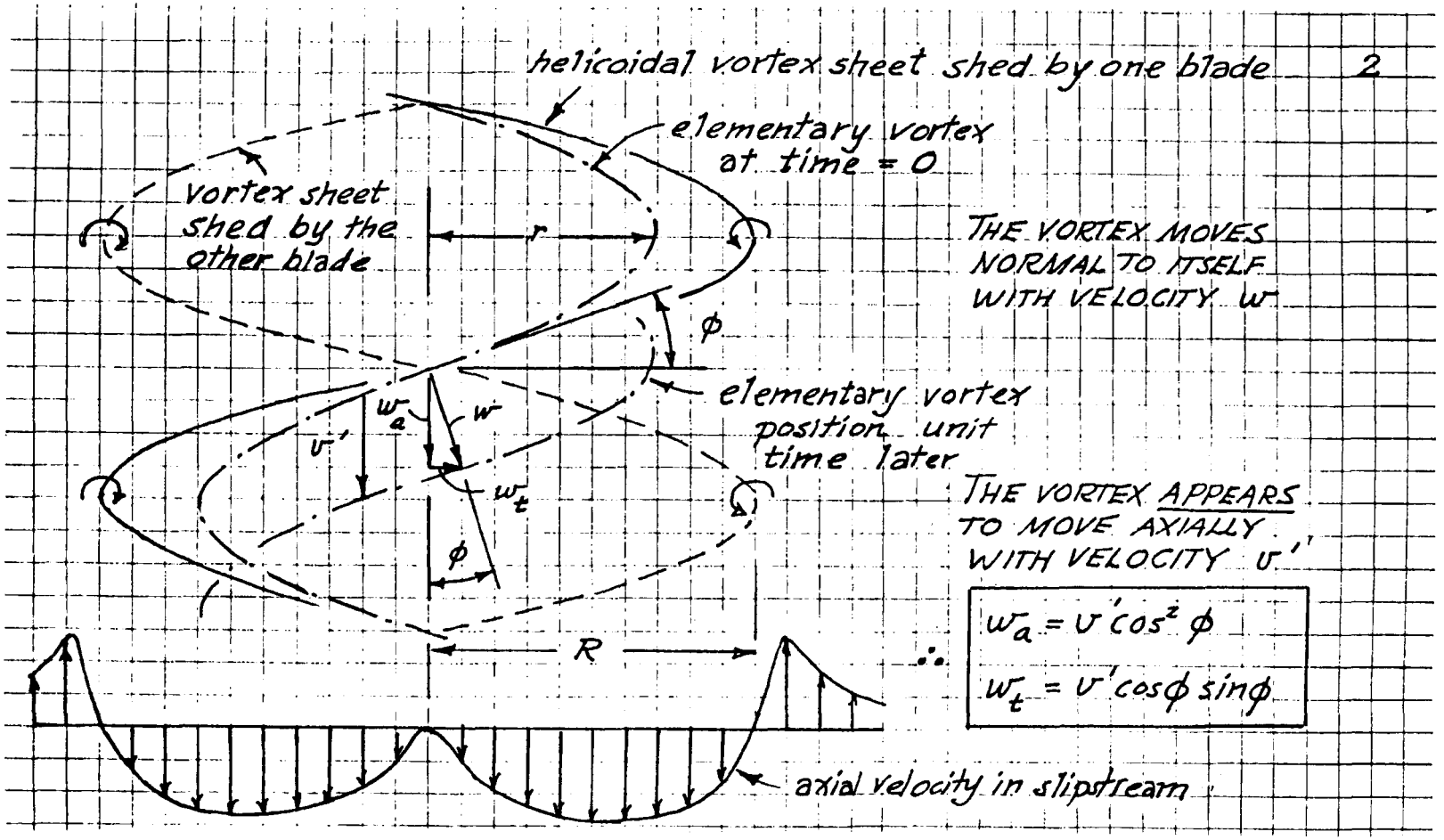

Figure 2. Propeller Slipstream Vortex Geometry

$$\tan\phi \cong \tan\phi_i \cong \frac{V}{\Omega r} \quad \begin{cases} \sin\phi = \dfrac{V}{\sqrt{V^2+\Omega^2 r^2}} \\ \cos\phi = \dfrac{\Omega r}{\sqrt{V^2+\Omega^2 r^2}} \end{cases}$$

in the slipstream

$$w_a = v'\cos^2\phi = v'\left(\frac{\Omega^2 r^2}{V^2+\Omega^2 r^2}\right)$$

$$w_t = v'\cos\phi\sin\phi = v'\left(\frac{V\Omega r}{V^2+\Omega^2 r^2}\right)$$

at the propeller

$$a = \frac{w_a}{2V} = \frac{1}{2}\left(\frac{v'}{V}\right)\left(\frac{\Omega^2 r^2}{V^2+\Omega^2 r^2}\right)$$

$$a' = \frac{w_r}{2\Omega r} = \frac{1}{2}\left(\frac{v'}{V}\right)\left(\frac{V^2}{V^2+\Omega^2 r^2}\right)$$

Figure 3. "Lightly Loaded" Propeller Relations

$$\eta_{induced} \equiv \frac{1-a'}{1+a} \cong \frac{1}{1+a+a'} = \frac{1}{1+\frac{1}{2}\left(\frac{v'}{V}\right)}$$

THE INDUCED EFFICIENCY FOR THE PROPELLER AS A WHOLE IS MAXIMIZED IF v'/V IS INDEPENDENT OF r

For a slipstream with "closely spaced" vortex sheets the circulation at radius r is

$$\Gamma_{total} = 2\pi r w_t$$

This is equal to the bound circulation on each of B blades at radius r (neglecting wake contraction) so that, for any blade

$$\Gamma(r) = \frac{2\pi r w_t}{B} = \left(\frac{2\pi v'}{B}\right) \frac{V\Omega r^2}{V^2+\Omega^2 r^2}$$

which may be written as

$$\left(\frac{B\Gamma\Omega}{2\pi V v'}\right) = \frac{\Omega^2 r^2}{V^2+\Omega^2 r^2} = \frac{x^2}{1+x^2}$$

where $x = \Omega r/V$

Figure 4. Betz's Minimum Induced Loss Condition (1919)

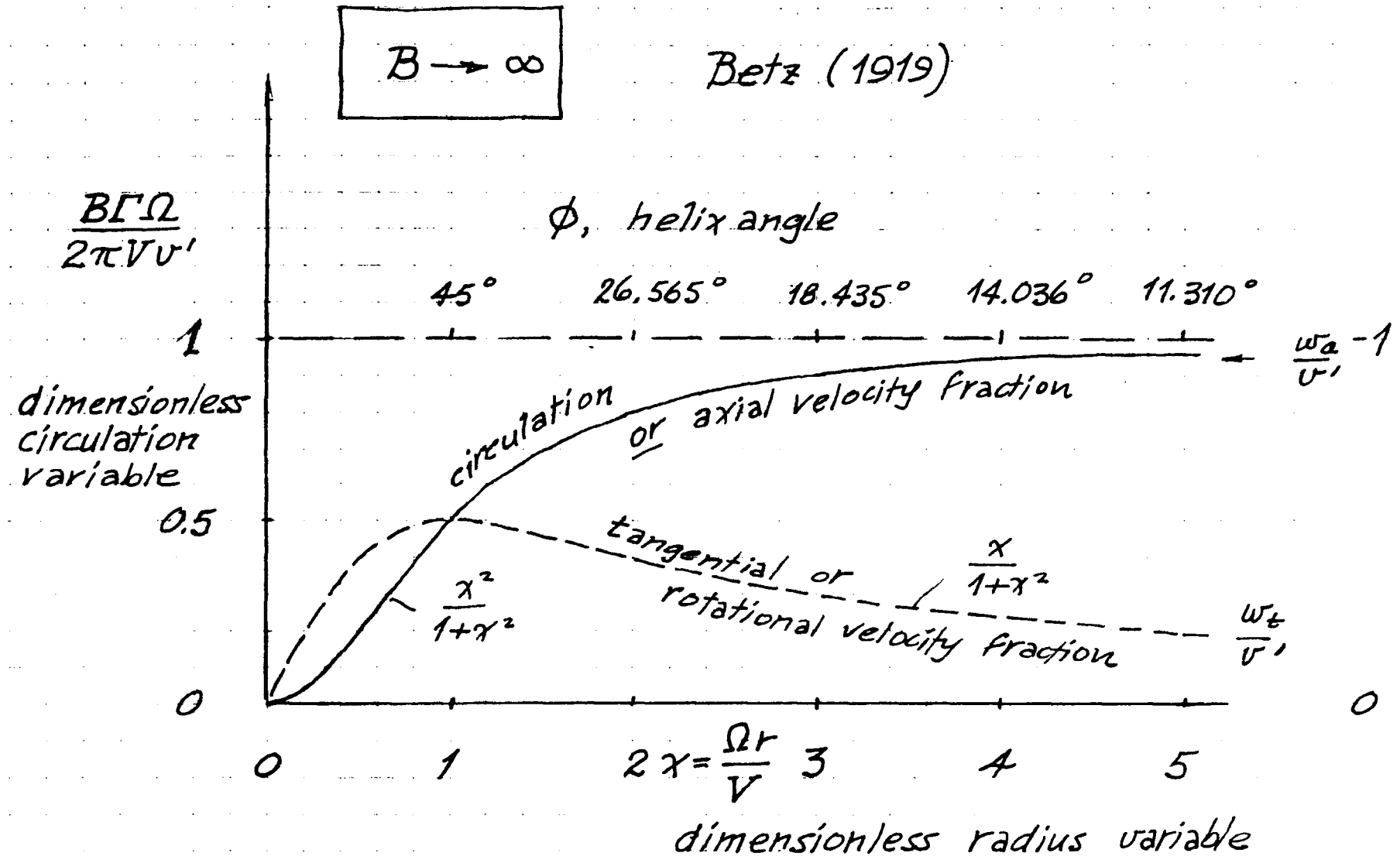

Figure 5. Radial Circulation Distribution for Minimum Loss

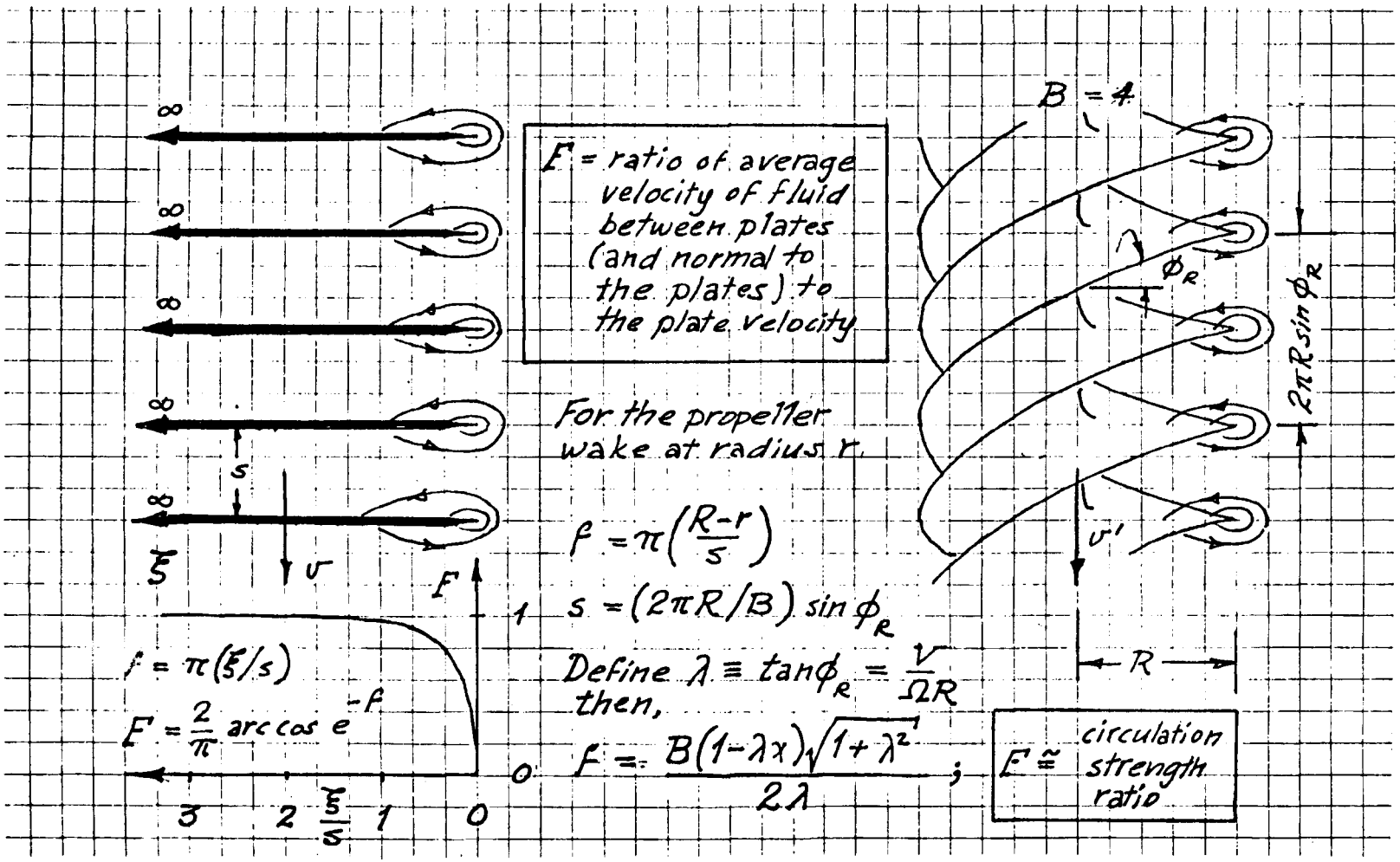

Figure 6. Prandtl's Vortex Sheet Spacing Correction (1919)

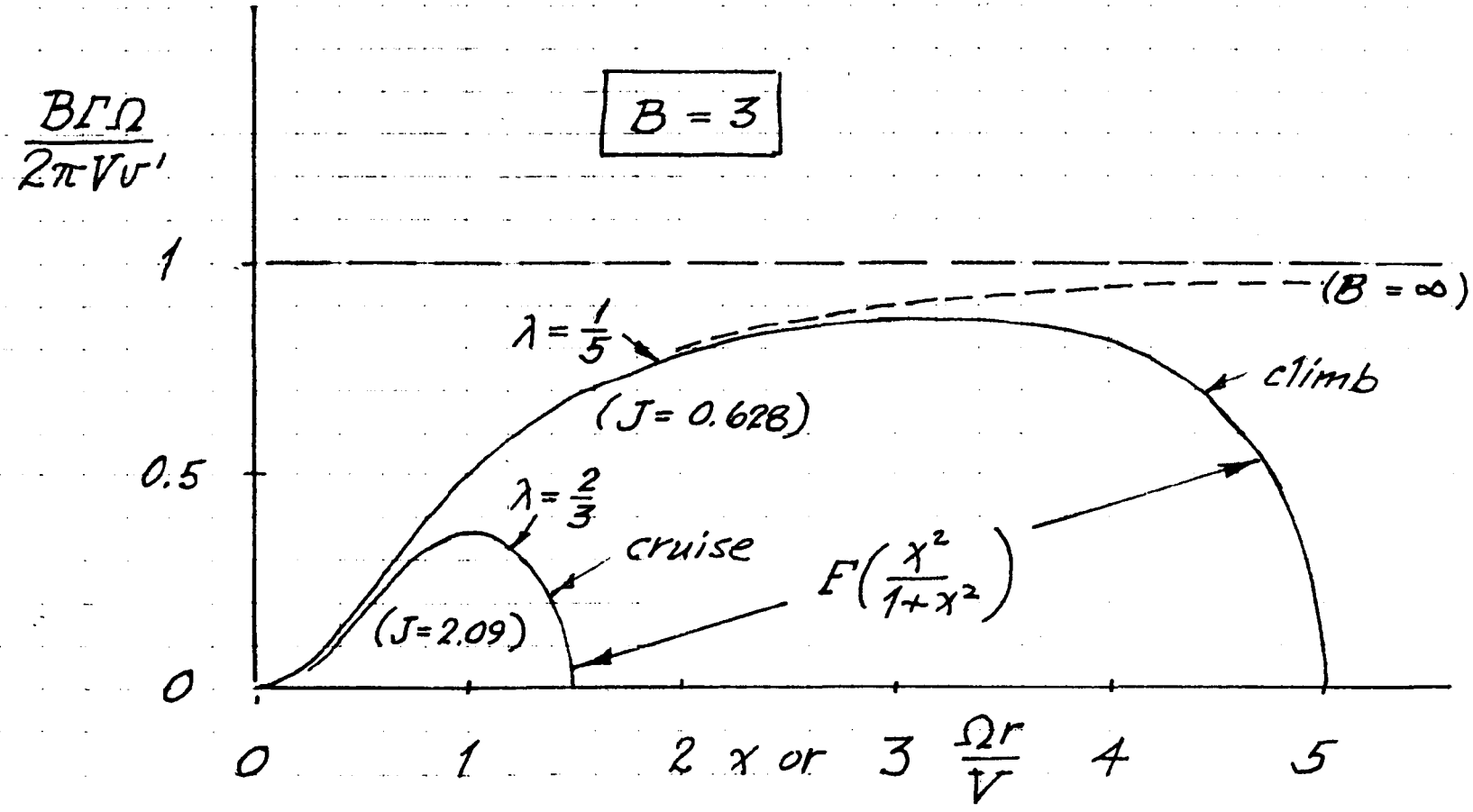

Figure 7. Typical Circulation Distributions for Minimum Induced Loss

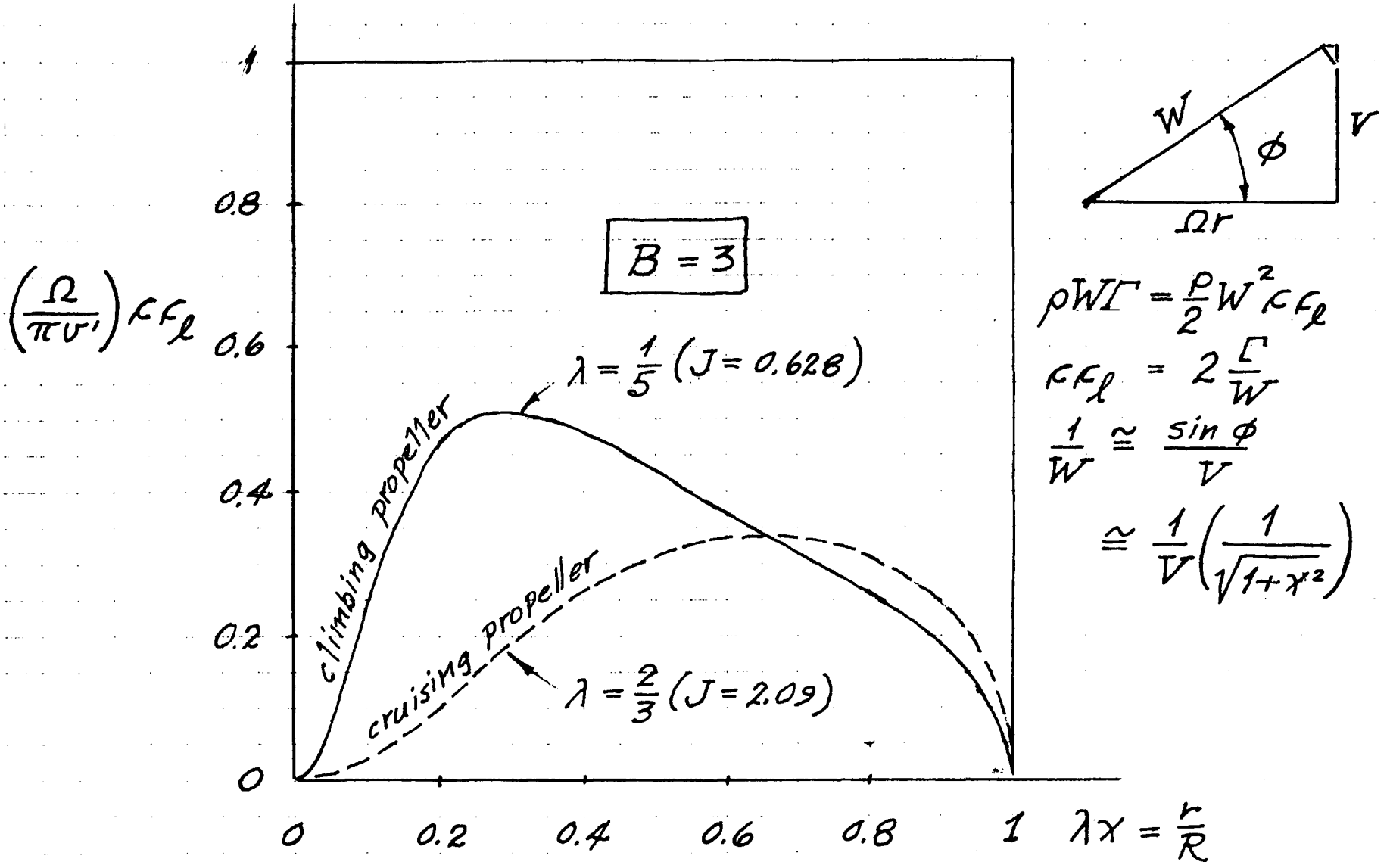

Figure 8. Typical Blade Chord Distributions for Minimum Induced Loss

Figure 9. Flow Visualization of a Two-Bladed Propeller
(Professor F.N.M. Brown's Propeller Smoke Picture - 1950)

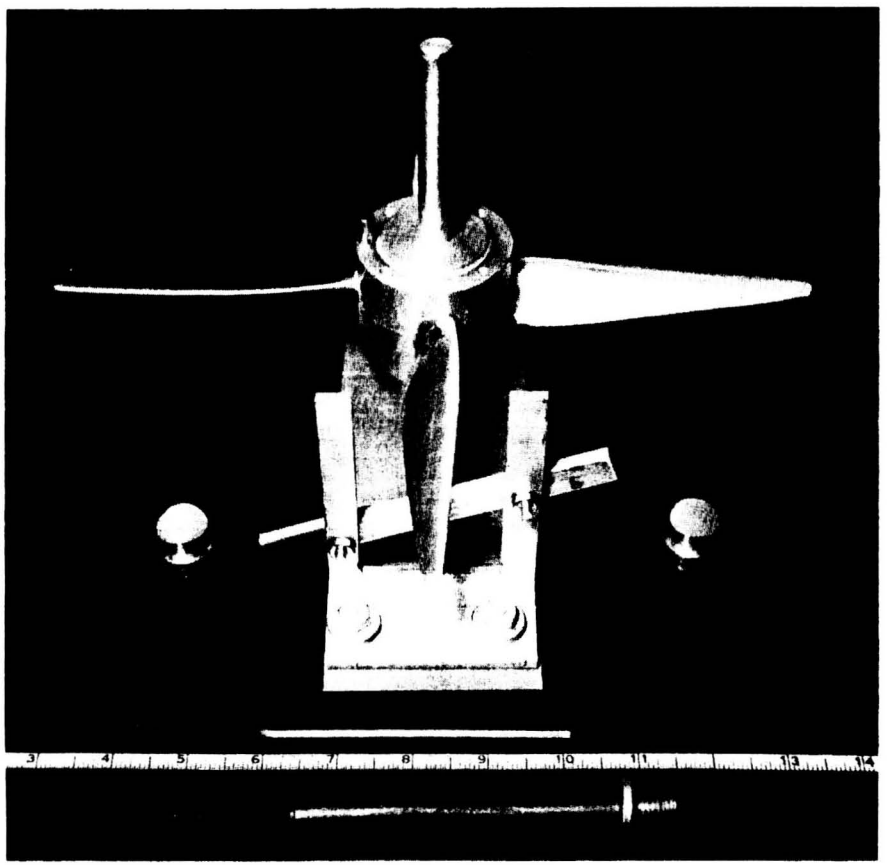

Figure 10. M.I.T. Research Propeller for Water Tunnel Tests

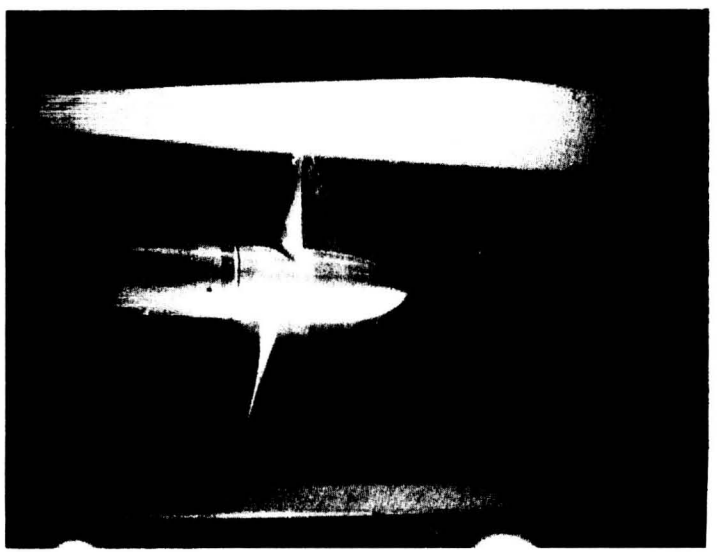

Figure 11. M.I.T. Research Propeller Operating Near Design Advance Ratio in Water Tunnel

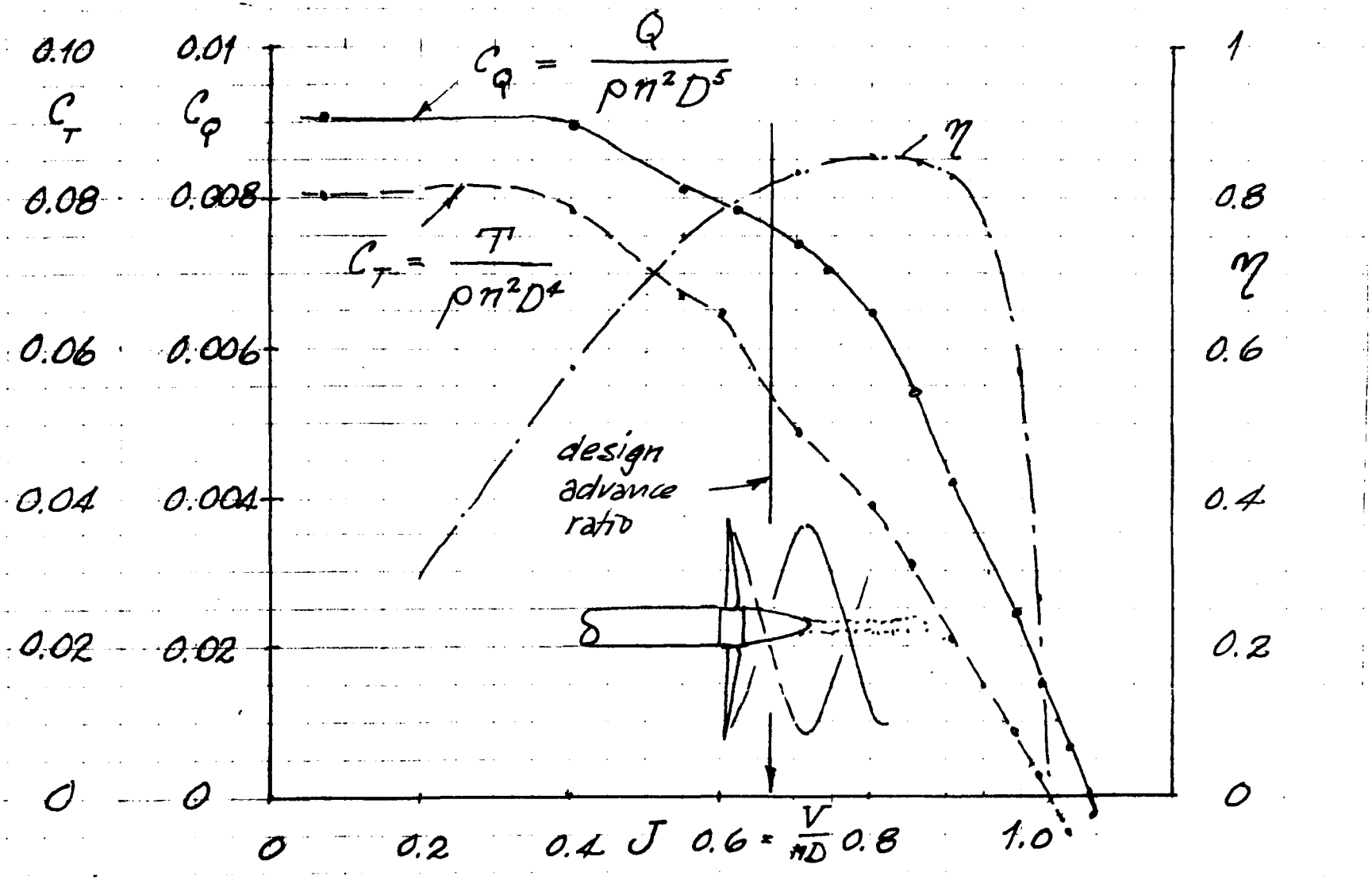

Figure 12. Water Tunnel Tests of a Minimum Induced Loss Propeller

7. PAPERS OF SESSION V - TRIM DRAG